

Design and optimization of bail-shaped microstrip patch antenna for mid-band 5G application using a lightGBM model

G. Vijayakumari¹, T. Annalakshmi²

¹Department of Electronics and Communications, New Prince Shri Bhavani College of Engineering and Technology, Chennai, India

²Department of Electronics and Communications, S. A. Engineering College, Chennai, India

Article Info

Article history:

Received Jun 3, 2025

Revised Sep 17, 2025

Accepted Oct 9, 2025

Keywords:

5G application

Bail-shaped microstrip patch antenna

High gain

Light gradient boosting machine optimization

Return loss

ABSTRACT

This study suggests a bail-shaped microstrip patch antenna designed for 5G applications. This antenna model operates in the 3.45 GHz wireless communication frequency range, which is a component of the so-called C-band (3.3 to 4.2 GHz), which is widely utilized for mid-band 5G deployments across the globe. Antenna size optimization is achieved at $31 \times 28 \text{ mm}^2$. On the patch, a slot is added to enhance the return loss features. The light gradient boosting machine (LightGBM) model for prediction acts as an objective function of the considered piranha foraging optimization algorithm (PFOA) to adjust the antenna's slot dimension, which will be used to optimize the slot width. In order to get a superior return loss value of around $-39.90 < -10 \text{ dB}$, the optimization approach that is provided seeks to achieve the ideal slot length. The proposed device exhibits remarkable radiation efficiency by partially grounding, with a peak gain of around 2.535 dBi at 3.45 GHz. A novel hybrid approach combines the LightGBM prediction model with the PFOA to fine-tune slot dimensions, achieving a superior return loss of -39.90 dB . The exclusivity of this effort is the incorporation of machine learning algorithms to attain significantly improved parameters.

This is an open access article under the [CC BY-SA](https://creativecommons.org/licenses/by-sa/4.0/) license.



Corresponding Author:

G. Vijayakumari

Department of Electronics and Communications Engineering

New Prince Shri Bhavani College of Engineering and Technology

Chennai, India

Email: varsisen@gmail.com

1. INTRODUCTION

The 5G technology is in high demand in the industry of wireless communication since it offers previously unheard-of connectivity and incredibly rapid data transfer speeds [1], [2]. 5G technology uses low-latency and high ratio frequencies to connect to numerous devices simultaneously [3]. This communication also improves the reliability and consistency of connections in crowded urban environments. Patch antennas' compact size, low profile, ease of integration, and multiband adaptability have made them more significant in modern wireless communication systems [4]. As a result, a patch antenna is created on a dielectric substrate that has several advantages due to its design. Patch antennas' low cost, ease of manufacture, and adaptability with a variety of form factors are some of their main advantages. This makes these antennas an excellent choice for use in wireless systems, internet of things (IoT) devices, and other small electronic devices [5]. Also, 5G networks will have to meet a number of performance requirements, including accurate frequency band coverage, high gain, and improved radiation efficiency. In order to achieve those requirements, a prior antenna arrangement had to overcome some obstacles. Finding an antenna with improved return loss behaviour at a given resonant frequency requires both optimal dimension

values and improved results. On the other hand, patch antennas pose some challenges since there exists no systematic process or precise mathematical formulas that guarantee precise solutions [6]. This technique covers machine learning (ML) and model of optimization models for implementing antenna design, thus to attain effective and optimum solutions [7], [8]. Furthermore, this in turn enables fine-tuning the parameters of antenna, thus attaining optimal performance metrics which could be complicated in attaining over traditional design iteration.

Traditional microstrip patch antennas for the application of 5G might be huge and thus less suitable for integrating them with compact devices [9]. Furthermore, conventional design methods may rely on laborious human or semi-automated optimization techniques. Without the sophisticated optimization scheme, it may be impossible to achieve ideal performance metrics like return loss and gain, which could lead to delayed designs. In order to construct an optimum patch antenna, this study uses an ML-dependent metaheuristic optimization model. In order to determine the ideal slot length for the proposed patch antenna and improve return loss values at 3.45 GHz (usually 3.3 to 4.2 GHz), a trained light gradient boosting machine (LightGBM) model will be used along with the objective function of the proposed piranha foraging optimization algorithm (PFOA).

2. LITERATURE REVIEW

González *et al.* [10] described design, implementation, simulation, and experimental results, and implementation of a wide bandwidth slotted planar microstrip patch antenna that spans from 3.1 GHz to 4.2 GHz. This work was applied to the initial trials along with the introduction of 5G services. The antenna that is being shown has a high bandwidth of 32% and a higher polarization purity. For the use of 5G, Ramasamy *et al.* [11] demonstrated a patch antenna on FR4 substrate. The recommended antenna operates in 5G n34 bands, WLAN at 5.2GHz, and Wi-max at 5.5GHz.

Ramasamy *et al.* [11] constructed a new millimeter-wave antenna array that operates at a incidence of 28 GHz for the 5G mobile communication system. This patch antenna has been rebuilt and features two U-shaped slots carved into the RT Rogers 5880 substrate. With an improved gain of 12 dB, the antenna design that is being shown achieves a radiation efficacy of almost 93%. The author of the paper introduced a 28 GHz microstrip patch antenna with a rectangular slot [12], [13]. An antenna with a height of 0.4 mm will be manufactured on a Rogers Rt-duroid substrate. According to an investigation, the gap-integrated feeding model was the best fit, satisfying the requirements for their use in 5G [14], [15].

A performance of microstrip patch antenna for varied substrates was estimated in the work [16]–[18]. A deep learning aided optimization strategy design was proposed for improving the performance of the antenna. A dual-band ultra-thin antenna appropriate for 5G applications will be designed. A presented model of an antenna occupies an area 30×30 mm², having a thickness of about 0.8 mm. This 28 GHz microstrip patch antenna is small, measuring 6.2×7.2 mm, and is intended for use with 5G networks. A designed antenna attains a return loss of about -26.40 dB with a bandwidth of 1.102 GHz. This in turn attains a gain value of 7.4 dB with an excellent voltage standing wave ratio (VSWR) of about 1.102 for the cellular 5G application. Defective ground structure (DGS) refers to the technique of controlling electromagnetic waves in an antenna by introducing intentional defects or disturbances in the ground plane [19].

Alfakhriet *et al.* [20] presented a compact, simple MIMO antenna that functions at UWB frequency band. The suggested antenna has four components, and the radiators' shape is derived from a number of adjustments made to a traditional rectangular patch antenna. A fractional bandwidth of 112% spanning from 3.1 GHz to 11 GHz was achieved, with a reflection coefficient below -10 dB and mutual coupling between antenna elements maintained below -20 dB. A lower antenna size and improved performance metrics indicate that the suggested antenna may find utility in a range of UWB applications, including portable handheld devices.

A non-uniform metasurface circularly polarized patch antenna design was proposed by Zeng *et al.* [21] using a real multi objective Bayesian optimization (MOBO) model. An optimized model attains an operating bandwidth of about 25.6% (3.75 to 4.85 GHz), having $|S_{11}| < -10$ dB, with an axial ratio lower than 3 dB with a maximal realized gain of 7.15 dBi. A better agreement between measurement and simulation outcomes validates optimization model.

Wang *et al.* [22] suggested A wearable dual-band planar inverted-F antenna (PIFA). In order to achieve wire band and dual band features, a design makes use of slots at the radiating plate with a ground plane. The prototype will be built and measured to confirm the design, and it will incorporate two operating bands of the application long range (LoRa), which are 433 MHz and 868 MHz. With a maximum gain of roughly 1.25 dBi, a proposed device offers a total radiation efficacy of roughly 70% across operating bands.

A novel tree-shaped Metamaterial microstrip antenna was introduced by Christydass *et al.* [23]. A suggested model structure measures a resistivity bandwidth of 45.39% with split-ring resonator (SRR) and 53.48% without SRR. The recommended antenna would satisfy the primary needs of contemporary wireless

devices, including multiband operation, small magnitude, high bandwidth, and two-dimensional structure. The presented model has sufficient impedance matching with small and wider bandwidth.

Several works have explored antennas for the communication of 5G; however, they might encounter some challenges like huge dimensions, low bandwidth impedance, or low gain that in turn affects the wireless communication quality [24], [25]. More research is needed to improve higher speed transmission of data ability. This suggested design seeks to optimize an antenna specifically tailored for cellular wireless communication applications. using ML techniques, with a focus on maximizing gains and decreasing return loss.

3. METHOD

The Bail-shaped microstrip patch antenna concept that has been suggested is shown in Figure 1. Figure 2 display the size of the antenna where Figure 2(a) shows the dimensions of the antenna (front view), and Figure 2(b) shows the back view of the antenna. This is then made up of the grounding layer, substrate, and radiating layers. The Rogers AD 450 (lossy) substrate will have a suggested antenna installed on it. The substrate's dielectric constant is 10.2 at a thickness of 1 mm. 5G communication systems are best suited for patch antennas with better permittivity and lower tangent dielectric loss because of their increased dependability and efficiency. Additionally, the substrate's thermal stability has been enhanced. As a result, they retain their electrical characteristics across a broad temperature range. Also, substrate offers better mechanical strength, thus making them suitable for the design of complex circuits that might involve in flexing or bending. The patch antenna's top surface comprises of single slot line having a thickness of 0.36 mm for enabling Bail-shaped operations. The proposed antenna is designed with a partially ground technique to improve the wider bandwidth and to tailor the gain and directivity. Also, this technique supports signal transmission efficiency by reducing return loss S_{11} .

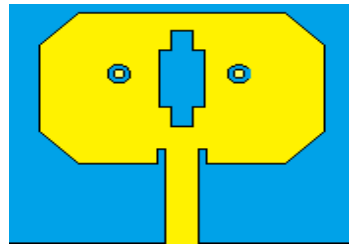


Figure 1. Bail-shaped microstrip patch antenna structure

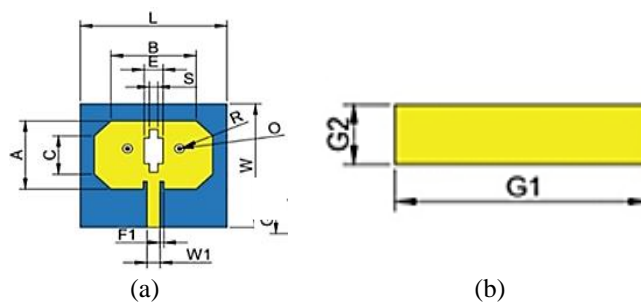


Figure 2. The structure and size of the proposed patch antenna with (a) front view showing the antenna dimensions, and (b) back view of the antenna

The intended frequencies for three operating bands can be created by cutting a 2.5 mm long slot in a radiating patch. 3 GHz, 4 GHz, and 4.2 GHz will be reached with a return loss value of roughly $-39.90 < -10$ dB, respectively. This improves the transmission efficiency and makes it appropriate for contemporary compact wireless communication. Table 1 shows the projected antenna's dimensions. The optimal slot length to enhance these return loss values is found using an optimization-based method in combination with the LightGBM model.

Table 1. Dimension of antenna

Parameter	Value (mm)
Patch length (A)	16
Patch width (B)	18
Substrate width (L)	31
Substrate length (W)	29
Diameter of slot (R)	4
Width of feed line (F1)	0.75
Length of feed line(W1)	2.8
Ground width (G1)	31
Ground length (G2)	8

3.1. Model development of piranha foraging optimization algorithm-lightGBM

This portion discusses inspiration and mathematical modeling of Piranha foraging optimization procedure:

$$x = \begin{bmatrix} x_{11} & x_{12} & x_{13} & \dots & x_{1D} \\ x_{21} & x_{22} & x_{23} & \dots & x_{2D} \\ \dots & \dots & \dots & \dots & \dots \\ x_{(n-1)1} & x_{(n-1)2} & x_{(n-1)3} & \dots & x_{(n-1)D} \\ x_{n1} & x_{n2} & x_{n3} & \dots & x_{nD} \end{bmatrix} \quad (1)$$

$x_i = [x_{i1} \ x_{i2} \ \dots \ x_{iD}]$ signifies position vectors, which signifies piranhas.

Accordingly, a PFOA identifies three patterns: hunting and scavenging forage, cluster attack, and limited grouping attack. Key stages include initializing and evaluating the population, then updating parameters and agent positions. The population set is expressed as:

- Step 1: initialization of population: initiate the position vectors for each individual in the population of piranha as per the following (2).

$$x_i = lb_i + \beta_1 \times (ub_i - lb_i) \quad (2)$$

In this, x_i signifies i th location of individual piranha candidate solution, ub_i and lb_i denotes upper and lower boundaries of piranha habitat search, correspondingly. β_1 denotes random number among 0 and 1.

- Step 2: define the parameter F for predation intensity: typically, Piranhas are sensitive tremendously top blood recognition, a feature which is influenced by concentration of blood F_1 and d_i distance among prey and piranhas. Piranhas mostly swim over the areas of higher blood concentration, fastens their movement, the higher the concentration of blood, and vice versa, [26] thus yielding following (3)-(5).

$$F_i = \beta_2 \times \frac{Z_i}{4\pi d_i^2} \quad (3)$$

$$d_i = x_{prey} - x_i \quad (4)$$

$$xZ_i = [x_i(t) - x_{i+1}(t)]^2 \quad (5)$$

Here, β_2 is a random value between 0 and 1, F_i is the predation intensity parameter for location with individual piranha, Z is the source intensity, and Z_i is the perceived source intensity from i th search agent that will alter in real time as agents continue to follow. D_i is the distance (best solution) between the position of the individual piranha and the prey.

- Step 3: strategies for non-linear parametric control: non-linear parametric control methods help smoothly balance exploration and exploitation. They are effective for handling changing random processes and help avoid early convergence of the population. In the early and middle stages of the PFOA algorithm, high values of S allow search agents to explore the global search space and avoid getting trapped in local optima using audit-based strategies. In contrast, later phases of this PFOA could converge quickly with changes in S , as (6) illustrates (6).

$$S = C \cdot \cos \left[\frac{\pi}{2} \otimes \left(\frac{t}{Max_Iter} \right) \right]^4 \quad (6)$$

Here, C is the confirmed constant (usually taken to be 5), and the maximum number of iterations is indicated by Max_Iter , \otimes which signifies the value of the product and variable.

- Step 4: the reverse escape search method: here, the 4-population search is redirected using flag E and the reverse escape search technique. This drives the examination to a new site and further enhances the solution by preventing the candidate population from becoming caught in the local area. Because it happens more frequently during the search process, search agents have more opportunities to carefully and thoroughly examine the search region, as illustrated in (7).

$$E = \begin{cases} 1 & \beta_3 \leq 0.5 \\ -1 & \beta_3 > 0.5 \end{cases} \quad (7)$$

In this β_3 signifies random number among 0 and 1.

- Step 5: Proxy formula location update
- i) A pattern of limited group attacks:

Like a group of foraging animals, this one may attack prey several times higher than itself when it is hungry. A splash of water is created when a prey enters the environment, and the piranha are alerted to the signal. The agent nearest to the prey attacks first as they quickly assemble to encircle and bite the victim. A mathematical model of a localized group attacking pattern will be shown in (8).

$$x_i(t+1) = \gamma_1 \sum_{k=1}^{pc} \frac{L_k(t) - x_i(t)}{pc} - x_{prey}(t) \quad (8)$$

Here, pc stands for randomly generated integers in SearchAgents_no. SearchAgents_no is the total number of agents, $x_i(t+1)$ is the new searching agent location, and $L_k(t)$ is the amount of local population fraction attacks that are achieved for the initial imitating attack, where $L \in X$, and X is the number of randomly generated piranhas. Whereas $x_{prey}(t)$ represents the location of the best agent discovered in a prior iteration, $x_i(t)$ indicates the location of the current agent. A random number, γ_1 , is evenly scattered between $[-2,2]$ and has a substantial influence on changing the piranhas' trajectory.

- ii) A bloodthirsty cluster attack pattern

Piranhas usually have a unique sensitivity for blood, are acutely aware of the blood's scent, and can detect when their prey is injured or bleeding. As a result, distant piranhas are drawn to the area of high blood concentration and begin attacking them violently. It can swim more quickly if its blood concentration is higher. The non-linear cosine factor, or S, which is influenced by E, blood concentration F_i , and the distance between piranhas and their prey, is the main determinant of this phase. Altering the movement of piranha direction could avoid local optima effectively, thus enabling them to identify better location of prey as shown in (9).

$$x_i(t+1) = \gamma_1 * e^{\gamma_2} * x_{prey}(t) + G * x_{prey}(t) + E * F_i + E * \beta_4 * S * F_i \quad (9)$$

Here, $x_i(t+1)$ is a search agent of new location, $x_{prey}(t)$ resembles best agent's location identified in previous iteration, γ_1 denotes random number that are distributed uniformly at $[-1/2,1/2]$ and β_4 signifies random number among 0 and 1. G signifies piranha's capacity for foraging, and it is an integer $G > 5$ (in this case, $G = 9$). $\gamma_1 * e^{\gamma_2}$ shows the uniform dispersion thus letting active alterations and trade-offs among local search & global search abilities.

- iii) Scavenging foraging patterns

Due to their poor vision, piranhas swim erratically to their habitat at night to feed on seeds and carrion, and they scatter from a group during forage in muddy watersheds. Vector analysis modelling is done by (10).

$$x_{i(t+1)} = \frac{1}{2} [e^{\gamma_2} * x_{C1}(t) - E * x_i(t)] \quad (10)$$

In this, $x_{i(t+1)}$ signifies search agents' new position, γ_2 denotes a random number that is distributed uniformly between $[-1,1]$, E denotes the parameter which alters the movement direction, $x_{C1}(t)$ indicates randomly selected closest agent position from piranhas, $x_i(t)$ indicates i^{th} position of the agent selected arbitrarily among agents, and $C1 \neq i$.

- iv) Survival strategy of Piranha population

Piranhas and their various natural predators have a reproductive trait that restricts the expansion of its population. In (11), it is used to determine the agent's survival rate (SR) in order to maintain population variety. The offspring population will be replicated once the SR falls below 1/4, indicating a decreased survival rate using (12).

$$SR(i) = \frac{fitness_{max} - fitness(i)}{fitness_{max} - fitness_{min}} \quad (11)$$

$$x_i(t + 1) = x_{prey}(t) + \frac{1}{2}\{[x_{C1}(t) - E * x_{C2}(t)] - [x_{C2}(t) - E * x_{C3}(t)]\} \tag{12}$$

In this, $x_i(t + 1)$ depicts newer position of the searching agent, $x_{prey}(t)$ resembles the best agent position identified in previous iteration, E indicates parameter to change direction and $x_{C1}(t)$, $x_{C2}(t)$, and $x_{C3}(t)$, signify agent positions C1, C2, and C3 selected randomly from piranhas with values $C1 \neq C2 \neq C3$ corresponding. The PFOA flowchart is revealed in Figure 3. This approach serves as an effective method for identifying optimum values, thus facilitating an effective search for optimal solutions at varied problem domains.

3.2. LightGBM model

LightGBM, a framework of gradient boosting, might be employed in optimizing the designs of antennas. Their scalability and efficiency for huge datasets make them suitable for tasks such as predicting the performance of an antenna or the parameters of optimization. This could be employed in training models that predict the performance of antennas depending on the design parameters, thus allowing them for effective design space exploration. LightGBM will be known for its higher accuracy, thus making them a reliable option for the optimization of antenna performance. This iterative process includes loss function minimization on adding newer models, which could complement deficiencies of traditional schemes.

A projecting model based on LightGBM was established to calculate return loss values for the slot radius (R) of a projected antenna at resonance frequencies of 3.45 GHz. PFOA employs the LightGBM model as its goal function to determine the optimal return loss parameters. 3 return loss yields that correspond to the designated frequency are produced by the LightGBM model using the slot radius as input. In essence, for a given radius R, the model predicts return loss values. The PFOA-LightGBM algorithm's consecutive phases are shown in Figure 4. In this approach, LightGBM's return loss predictions serve as the fitness function in the PFOA. During both exploration and exploitation, LightGBM predictions guide the selection of better candidate solutions for slot radius. The fitness function evaluates how well a particular radius enhances return loss at the desired frequencies.

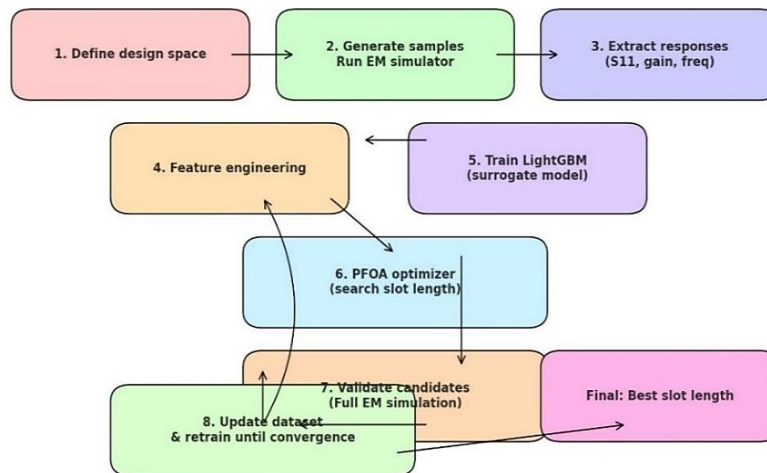


Figure 3. Flowchart of PFOA+lightGBM model

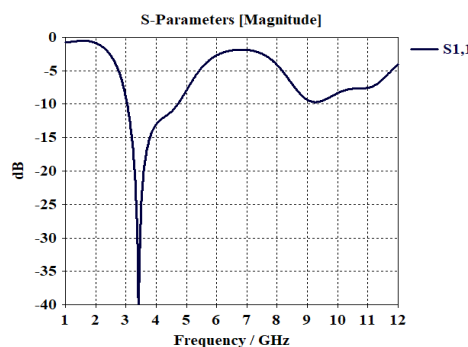


Figure 4. S11 plot for proposed antenna

4. RESULTS

This section delivers the results estimated for the proposed bail-shaped microstrip antenna design. Figure 4 shows the S-parameter (S11) magnitude response of the device over a frequency range that ranges from 1 GHz to 12 GHz. The S11 parameter, plotted in red, signifies the input reflection coefficient in dB. The clear resonance is observed approximately at 3.42 GHz at which S11 magnitude reaches a minimal value of -39.9 dB, thus indicating excellent matching and minimal reflection at this frequency. A deep null suggests that the device is well matched at 3.42 GHz, thus making it an ideal operating frequency for the antenna. Beyond resonance, S11 value increases with notable variation over a frequency range, thus indicating varied impedance matching performance at varied frequencies.

Figure 5 is the power distribution over varied categories as a function of frequency that ranges from 1 GHz to 12 GHz. A loss in dielectrics, loss in metals, power absorbed at all ports, power accepted, outgoing power at ports, and simulated power are estimated and are shown in varied colors. The plot shows that the device exhibits maximum radiation efficiency around 3.4 GHz, correlating with strong impedance as shown in S11 plot. The losses remain minimal over all materials, thus emphasizing effective design.

Figure 6 shows a polar representation of the far-field electric field radiation pattern in the E-plane. ($\Phi=90^\circ$) at frequencies 6(a) 3 GHz, 6(b) 4 GHz, and 6(c) 4.2 GHz correspondingly. Electric field strength of the main lobe in decibels relative to 1 V/m. $17.2 \text{ dB(V/m)} \approx 6.48 \text{ V/m}$ (linear scale). This is adequate for typical line-of-sight (LOS) 5G applications, especially in urban or suburban scenarios. The main beam is directed at 176 degrees in the azimuth plane, nearly due south. Directionality is essential for beamforming, sectorized coverage, and spatial reuse in 5G. A beamwidth of 90.5° is relatively wide, indicating a broad coverage area. This outcome confirms consistent far-field performance and directionality over 3-4.2 GHz range having slight enhancement in the radiated strength at 4.2 GHz.

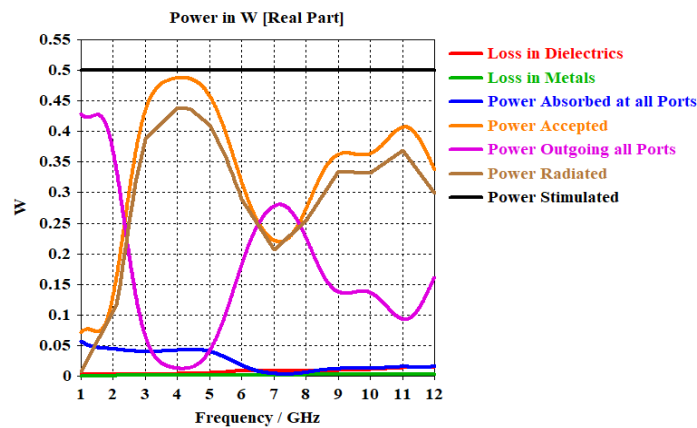


Figure 5. Power estimated representation in W

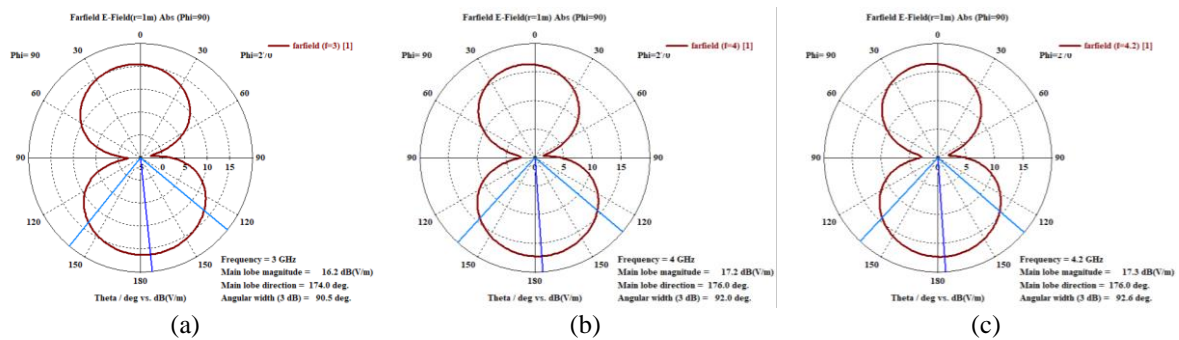


Figure 6. E-field: (a) 3 GHz, (b) 4 GHz, and (c) 4.2 GHz

Figure 7 shows the 3D radiation pattern (directivity) at 3 GHz, Figure 7(a) thus showing the directivity distribution of the far-field electric field. The radiation pattern is nearly omnidirectional in the Phi plane with clear symmetry around the Z axis. The structure radiates more efficiently horizontally in (theta

plane), typical of dipole-like antennas. It indicates a moderately directive antenna having good efficiency at which most of the power is radiated in the horizontal plane. Figure 7(b) shows the 3D radiation pattern (directivity) at 4 GHz, thus showing the directivity distribution of the far-field electric field. The radiation pattern is broadly omnidirectional in the horizontal theta plane with clear symmetry around Z axis, thus resembling a doughnut-shaped pattern. The antenna exhibits efficient radiation having moderate directivity, thus maintaining wide angular coverage.

Figure 7(c) shows the 3D radiation pattern (directivity) at 4.2 GHz, thus showing the directivity distribution of the far-field electric field. The radiation pattern is broadly omnidirectional in the horizontal theta plane with clear symmetry around the Z axis, thus resembling a consistent doughnut-shaped pattern. At this range, the antenna continues to deliver effective performance with stable radiation characteristics. Figure 8 is the estimation of VSWR plot as a function of frequency, which is a key metric to estimate the impedance of the antenna over a frequency range. This plot confirms that the antenna is optimized for the function near 3 GHz, aligning well with the radiation pattern outcome attained as shown before. Figure 9 displays the Z-parameter (impedance) magnitude plot of the antenna system over the frequency range of 1 GHz to 12 GHz. The plot confirms that the antenna design or system is matched optimally around 3 GHz, and is 50 ohm. Figure 10 shows the maximum gain estimation over frequency, a performance indicator of antenna efficiency and directionality over a broad frequency range (1 GHz to 12 GHz). An optimal gain performance is attained from 3 GHz as 2.5 dB, 4 GHz (2.5 dB), 4.2 GHz (2.8 dB), and a maximum of 5.4 dB gain at 8 GHz.

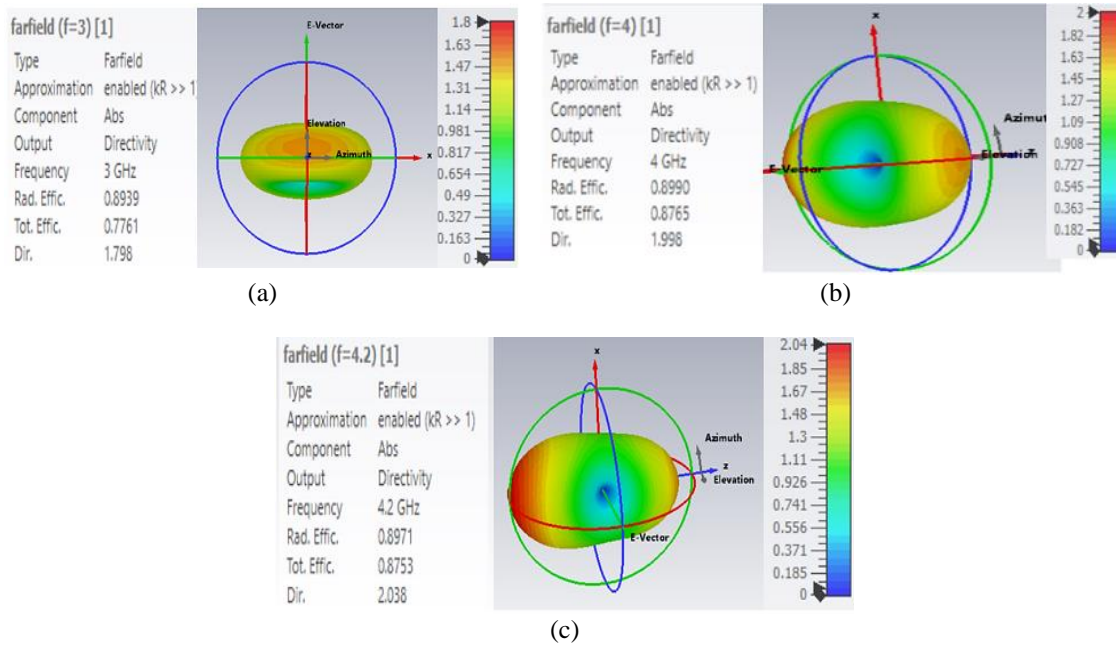


Figure 7. Directivity at (a) 3GHz, (b) 4 GHz, and (c) 4.2 GHz

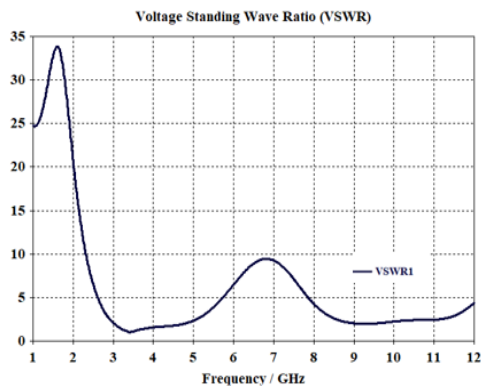


Figure 8. VSWR estimation

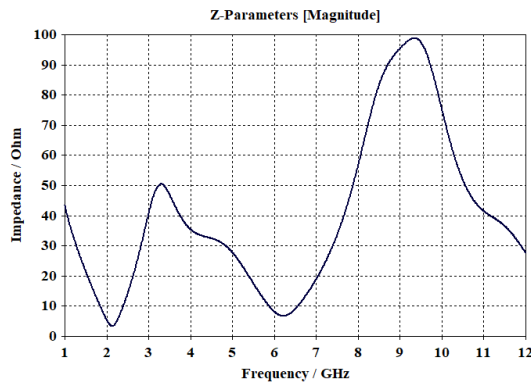


Figure 9. Estimation of impedance

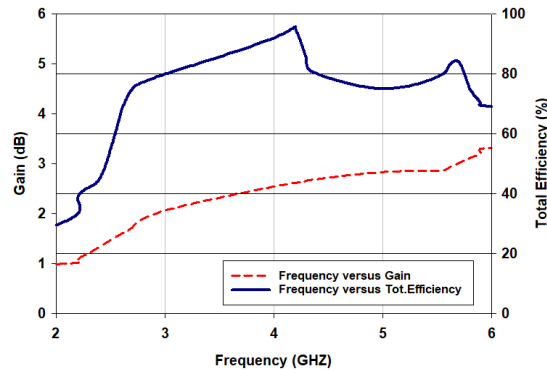


Figure 10. Gain vs frequency estimation plot

5. DISCUSSION

Figure 11 shows a fabricated bail-shaped patch antenna. Figure 12 shows an antenna connected with VNA to measure the antenna parameters. Figure 13 displays a graph titled "simulated vs measured," plotting the S11 parameter (in dB) of an antenna against frequency (in GHz). The graph shows two curves: a solid blue line represents the simulated S11, while a dashed red line denotes the measured S11. The measured results (red dashed line) generally follow the trend of the simulated results, showing a significant dip in S11 around 3.7 GHz, reaching a value of roughly -38 dB. This indicates that the fabricated antenna's resonant frequency is closely related to higher compared to the simulation. The suggested antenna design is contrasted with alternative design methodologies in Table 2. The proposed antenna design achieves a gain of 2.535 dBi, outperforming other models and minimizing power loss.



Figure 11. Fabricated bail-shaped microstrip patch antenna



Figure 12. Proposed antenna connected with VNA to measure the S11 parameter

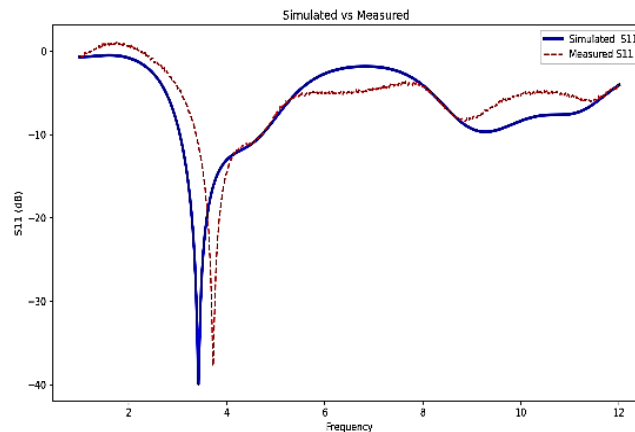


Figure 13. S11 parameters measured vs simulated

Table 2. Comparison of proposed antenna design

References	Size (mm)	Substrate material	Technique used	Operating frequency (GHZ)	S11 (dB)	Gain (dBi)
[7]	44x12	FR-4	Partial ground	3.1-4.2	<-10	-
[17]	48x44x1.6	FR-4	Defected ground structure	3.1-11	<-20	4.7
[18]	$1.12\lambda_0 \times 0.86\lambda_0$ $0.069\lambda_0$	FR-4	Circularly polarized	3.75-4.85	<-10	7.15
[19]	$0.12\lambda_0 \times 0.25\lambda_0$	Textile	PIFA	4.3-8.68	<-10	1.25
[20]	16x15	FR-4	Partial ground	5.5-10.72	-23.73 -12.01	1.35
Proposed work	29x31x1	Roger 350	Partial ground	3.4 (3.01-4.7)	-39.90<-10	2.535

Table 3, besides Figure 14 shows the evaluation of prediction accuracy of various existing models and proposed model employed for antenna design. The existing models like random forest, Gaussian process regression, neural network, XGBoost are compared with proposed (PFOA+LightGBM) model. The analysis shows the proposed model achieves higher prediction accuracy (about 98.6%) compared to existing schemes, demonstrating strong capability in assessing accuracy across varied slot widths. However, the LightGBM model is more complex to tune and less intuitive than other methods, with challenges in scalability and sensitivity for large, complex designs.

Table 3. Performance comparison of proposed scheme

Types of models	Prediction accuracy [%]
Random forests	89.5
Gaussian process regression	91.6
Neural networks	93.5
XG Boost	96.4
Proposed (PFOA+LightGBM)	98.6

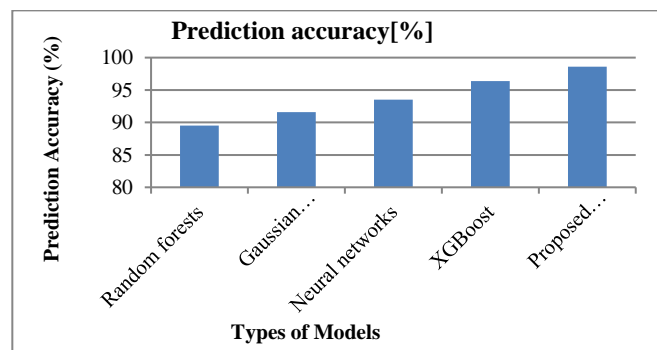


Figure 14. Performance comparison of prediction accuracy





6. CONCLUSION

A design development and optimization of a bail-shaped microstrip patch antenna was essential for attaining improved 5G wireless connection performance. In order to improve performance, a new hybrid model based on machine learning and metaheuristic optimization was created in this study for constructing a microstrip patch antenna. The presented LightGBM model is identified to be the suitable one on comparing other ML models for performance comparison. The antenna designed resonates at frequency range of 3.45 GHz, having a return loss of $-39.90 < -10$ dB correspondingly. A higher gain value of about 2.535 dBi is attained for proposed design. The outcome simulated shows a better outcome in relation to radiation pattern, field distribution, VSWR, and so on. An antenna designed is a suitable choice for the application of 5G technology, specifically in the case of a high gain need. The developed antenna's outcomes are quite satisfactory and suit quite fine with 5G communication. Future work could focus on integrating advanced optimization or deep learning models to automate antenna dimension tuning and reduce noise for practical 5G communication.





REFERENCES

- [1] K. Sandeep, N. Sharma, and N. Narawade, "High-isolation dual-band slotted patch MIMO antenna for sub-6 GHz 5G applications," *International Journal of Advanced Technology and Engineering Exploration*, vol. 12, no. 123, pp. 301–316, 2025, doi: 10.19101/IJATEE.2024.111100612.
- [2] K. Mamta and R. K. Singh, "Miniaturized novel quintuple-band microstrip patch antenna for K-band application," *International Journal of Advanced Technology and Engineering Exploration*, vol. 11, no. 113, pp. 501–515, 2024, doi: 10.19101/IJATEE.2023.10102106.
- [3] X. H. Ding, Z. Tan, and S. N. Burokur, "A compact single layer dual band microstrip patch antenna for 5G terminal applications," *Scientific Reports*, vol. 15, no. 1, p. 8601, Mar. 2025, doi: 10.1038/s41598-025-93592-3.
- [4] R. Ganesan, M. V. Panchavarnam, and J. Thangaiyan, "Split Ring Resonator Inspired Dual-Band Monopole Antenna for ISM, WLAN, WIFI, and WiMAX Application," *Tehnicki Vjesnik*, vol. 30, no. 5, pp. 1533–1538, Oct. 2023, doi: 10.17559/TV-20230210000344.
- [5] M. Alagarsamy, V. Mathiyazhagan, D. P. Mani, M. Chitrakannu, B. V. L. Kannan, and K. Suriyan, "Circular slot antenna for triband application," *International Journal of Reconfigurable and Embedded Systems*, vol. 11, no. 3, pp. 226–232, Nov. 2022, doi: 10.11591/ijres.v11.i3.pp226-232.
- [6] A. Li and K. M. Luk, "Single-Layer Wideband End-Fire Dual-Polarized Antenna Array for Device-to-Device Communication in 5G Wireless Systems," *IEEE Transactions on Vehicular Technology*, vol. 69, no. 5, pp. 5142–5150, May 2020, doi: 10.1109/TVT.2020.2979636.
- [7] C. Sun, Z. Wu, and B. Bai, "A Novel Compact Wideband Patch Antenna for GNSS Application," *IEEE Transactions on Antennas and Propagation*, vol. 65, no. 12, pp. 7334–7339, Dec. 2017, doi: 10.1109/TAP.2017.2761987.
- [8] H. Ozpinar, S. Aksimsek, and N. T. Tokan, "A Novel Compact, Broadband, High Gain Millimeter-Wave Antenna for 5G Beam Steering Applications," *IEEE Transactions on Vehicular Technology*, vol. 69, no. 3, pp. 2389–2397, Mar. 2020, doi: 10.1109/TVT.2020.2966009.
- [9] Ruchi, A. Patnaik, and M. V. Kartikeyan, "Compact dual and triple band antennas for 5G-IOT applications," *International Journal of Microwave and Wireless Technologies*, vol. 14, no. 1, pp. 115–122, Feb. 2022, doi: 10.1017/S1759078721000301.
- [10] S. R. M. González and R. T. R. Márquez, "Microstrip Antenna Design for 3.1–4.2 GHz Frequency Band Applied to 5G Mobile Devices," *European Journal of Engineering and Technology Research*, vol. 4, no. 10, pp. 111–115, Oct. 2019, doi: 10.24018/ejeng.2019.4.10.1570.
- [11] E. Suganya, T. A. J. M. Pushpa, and T. Prabhu, "Advancements in Patch Antenna Design for Sub-6 GHz 5G Smartphone Application: A Comprehensive Review," *Wireless Personal Communications*, vol. 137, no. 4, pp. 2217–2252, Aug. 2024, doi: 10.1007/s11277-024-11484-7.
- [12] G. K. Michelon, W. K. G. Assuncao, P. Grunbacher, and A. Egyed, "Analysis and Propagation of Feature Revisions in Preprocessor-based Software Product Lines," in *Proceedings - 2023 IEEE International Conference on Software Analysis, Evolution and Reengineering, SANER 2023*, IEEE, Mar. 2023, pp. 284–295, doi: 10.1109/SANER56733.2023.00035.
- [13] S. Ramasamy and A. Madhu, "A compact tri-band MIMO antenna for WLAN and 5G applications," *Applied Physics A: Materials Science and Processing*, vol. 130, no. 2, p. 113, Feb. 2024, doi: 10.1007/s00339-023-07249-x.
- [14] K. M. Mak, H. W. Lai, and K. M. Luk, "Communication A 5G Wideband Patch Antenna with Antisymmetric L-shaped Probe Feeds," *IEEE Transactions on Antennas and Propagation*, vol. 66, no. 2, pp. 957–961, Feb. 2018, doi: 10.1109/TAP.2017.2776973.
- [15] A. Zhang, K. Wei, Y. Hu, and Q. Guan, "High-Isolated Coupling-Grounded Patch Antenna Pair with Shared Radiator for the Application of 5G Mobile Terminals," *IEEE Transactions on Antennas and Propagation*, vol. 70, no. 9, pp. 7896–7904, 2022, doi: 10.1109/TAP.2022.3168276.
- [16] K. R. Mahmoud and A. M. Montaser, "Performance of tri-band multi-polarized array antenna for 5G mobile base station adopting polarization and directivity control," *IEEE Access*, vol. 6, pp. 8682–8694, 2018, doi: 10.1109/ACCESS.2018.2805802.
- [17] U. Ullah, M. Al-Hasan, S. Koziel, and I. Ben Mabrouk, "A Series Inclined Slot-Fed Circularly Polarized Antenna for 5G 28 GHz Applications," *IEEE Antennas and Wireless Propagation Letters*, vol. 20, no. 3, pp. 351–355, 2021, doi: 10.1109/LAWP.2021.3049901.
- [18] R. M. Moreno, J. Ala-Laurinaho, A. Khripkov, J. Ilvonen, and V. Viikari, "Dual-polarized mm-wave endfire antenna for mobile devices," *IEEE Transactions on Antennas and Propagation*, vol. 68, no. 8, pp. 5924–5934, 2020, doi: 10.1109/TAP.2020.2989556.
- [19] P. Liu, X. W. Zhu, Y. Zhang, X. Wang, C. Yang, and Z. H. Jiang, "Patch Antenna Loaded with Paired Shorting Pins and H-Shaped Slot for 28/38 GHz Dual-Band MIMO Applications," *IEEE Access*, vol. 8, pp. 23705–23712, 2020, doi: 10.1109/ACCESS.2020.2964721.
- [20] A. Alfakhri, "Dual polarization and mutual coupling improvement of UWB MIMO antenna with cross shape decoupling structure," *e-Prime - Advances in Electrical Engineering, Electronics and Energy*, vol. 4, 2023, doi: 10.1016/j.prime.2023.100130.
- [21] Y. Zeng, X. Qing, and M. Y. W. Chia, "A Wideband Circularly Polarized Antenna with a Nonuniform Metasurface Designed via Multiobjective Bayesian Optimization," *IEEE Antennas and Wireless Propagation Letters*, vol. 23, no. 6, pp. 1739–1743, 2024, doi: 10.1109/LAWP.2024.3368030.
- [22] X. Wang, L. Xing, and H. Wang, "A wearable textile antenna for LoRa applications," *2021 IEEE 4th International Conference on Electronic Information and Communication Technology, ICEICT 2021*, pp. 613–615, 2021, doi: 10.1109/ICEICT53123.2021.9531121.
- [23] S. P. J. Christydass *et al.*, "Design of Metamaterial Antenna Based on the Mathematical Formulation of Patch Antenna for Wireless Application," *International Journal of Antennas and Propagation*, vol. 2023, 2023, doi: 10.1155/2023/2543923.
- [24] J. A. Aldhaibani, M. Q. Mohammed, A. A. Mahmood, and M. S. Hamza, "Development of wearable textile patch antenna 2.43 GHz for biomedical applications," *International Journal of Advanced Technology and Engineering Exploration*, vol. 11, no. 111, pp. 177–189, 2024, doi: 10.19101/IJATEE.2023.10102312.
- [25] G. Kartikasari, M. P. K. Praja, and S. Romadhona, "Design of Rectangular Patch Microstrip Antenna with Defected Ground Structure Method at 3.5 GHz Frequency for 5G Technology," *Journal of Information Technology and Its Utilization*, vol. 6, no. 2, pp. 79–85, 2023, doi: 10.56873/jitu.6.2.5259.
- [26] S. Cao, Q. Qian, Y. Cao, W. Li, W. Huang, and J. Liang, "A Novel Meta-Heuristic Algorithm for Numerical and Engineering Optimization Problems: Piranha Foraging Optimization Algorithm (PFOA)," *IEEE Access*, vol. 11, pp. 92505–92522, 2023, doi: 10.1109/ACCESS.2023.3267110.

BIOGRAPHIES OF AUTHORS

G. Vijayakumari     received a B.E. degree in Electronics and Communication Engineering and M.E. in Applied Electronics from Anna University in 2005 and 2013 respectively. Currently working towards Ph.D. degree with the Department of Electronics and Communication Engineering, S.A. Engineering College, Chennai, India. She is currently working as assistant professor in the Department of Electronics and Communication Engineering., New Prince Shri Bhavani College of Engg. and Tech., Chennai. Her area of interest is antenna, wave propagation, and wireless communication. She is a life member of IETE, ISTE, and IAENG. She can be contacted at email: varsisen@gmail.com.



T. Annalakshmi     received the B.Tech. degree in Electronics and Communication Engineering from Pondicherry University in 2002 and M.E. degree in Communication Systems in 2011 and Ph.D. Degree in the Department of Electronics and Communication Engineering, from Anna University in 2023. She is currently working as associate professor in the Department of Electronics and Communication Engineering, S.A. Engineering College with experience of 17 Years. She authored papers in reputed journals and international conferences. Her area of research interest includes antenna and wave propagation and wireless communication. She is guiding research scholars in the field of antenna design and wireless communication. She is a life member of ISRD and ISTE. She can be contacted at email: lakshmishanmu15@gmail.com.